



Inverse neural networks modelling of a piezoelectric stage with dominant variable

Gangfeng Yan¹

Received: 15 January 2021 / Accepted: 5 July 2021 / Published online: 15 July 2021
© The Brazilian Society of Mechanical Sciences and Engineering 2021

Abstract

This paper presents an approach for developing a neural network inverse model of a piezoelectric positioning stage, which exhibits rate-dependent, asymmetric hysteresis. Unlike most piezoelectric actuators being investigated, the stage involves sliding motion with a maximum range of travel of over 10cm and, therefore, frictional disturbances are significant. The proposed inverse model is a feedforward neural network trained using the Levenberg–Marquardt algorithm. Such a static network is capable of modelling the dynamic features of the hysteresis using the velocity signals. However, using both the velocity and the acceleration as inputs results in overfitting. With a rough analytical model of the actuator and by measuring its response to excitation, velocity was identified as the dominant variable. By setting the input space of the neural network to only this dominant variable, an inverse model with good predictive ability is obtained. Its effectiveness in feedforward compensation for position control is experimentally demonstrated by tracking the positioning reference signal with an amplitude of 20 mm and a period of 0.5 and 1 Hz, respectively.

Keywords Neural network modelling · Dominant variable · Complex nonlinearity · Piezoelectric positioning stage · Model-based control

1 Introduction

Piezoelectric actuators are an attractive choice for high precision micro-positioning applications due to their quick response time, large force output, and high bandwidth. Example application areas include atomic force microscopes [1, 2], adaptive optics [3], and computer components [4]. Regarding the standard stack or bender piezoelectric actuators used in nano-positioning, Mohammadzaheri et al [5] give a detailed overview of the characteristics of the piezoelectric actuators and their applications and suggest future trends of nano-positioning.

The inherent nonlinear nature of piezoelectric actuators means that their full capabilities can only be realised with careful control [6], but this is challenging due to the

complexity of the nonlinearity, which is a combination of hysteresis and creep phenomena. Nevertheless, many advanced control methods have been successfully applied to piezoelectric actuators (see [7]). On the other hand, the standard control strategy of combining feedforward and feedback control is simple and feasible [8], but to attain high precision, an accurate actuator model (or its inverse) is needed for feedforward compensation. As hysteresis is the dominant source of error in piezoelectric actuators (the creep effect occurs over a longer timescale), much work has focused on modelling it accurately. The key issue in modelling hysteresis is how to adequately describe its dynamical nature. In other words, knowledge of the current input is insufficient; some idea of its past is necessary as well. In a sense, this is a problem of transforming a multi-valued mapping into a one-to-one mapping. Matters are complicated by the asymmetry and rate-dependence of the hysteresis [9].

Since physics-based models are hard to derive and only narrowly applicable, most available models are phenomenological. The applicability of phenomenological models across different physical systems, such as in the magnetisation of materials and the displacements generated by shape memory alloys, makes it possible to draw

Technical Editor: Monica Carvalho.

✉ Gangfeng Yan
scuygf@163.com

¹ College of Electronic Information and Electrical Engineering, Chengdu University, Chengdu 610106, Sichuan, China

from hysteresis modelling work in those areas. However, parameter estimation for phenomenological models may be less straightforward compared to physical models, if parameters do not directly correspond to physically measurable quantities. Hassani et al give a recent review [10] of many analytical models of hysteresis, which they broadly categorise as involving either the use of hysteretic operators, or differential equations. The classic Preisach model and the Krasnoselskii-Pokrovskii model are representative of the operator approach, where complicated hysteresis models are constructed by the superposition of elementary hysteresis operators. Using more of these building blocks increases the precision of the model, but also the number of parameters that need to be estimated. For the purpose of feedforward compensation an inverse hysteresis model is typically required. The Preisach and Krasnoselskii-Pokrovskii models are not amenable to analytic inversion, although numeric inversion is possible [11]. The Prandtl-Ishlinskii (P-I) model overcomes this difficulty, and its inverse has been successfully employed for feedforward compensation in a piezoelectric actuator [12].

Since hysteretic behaviour depends on the past state of the system, it is natural to consider the use of differential equations for modelling hysteresis. The Bouc-Wen model is one such model which has been applied to piezoelectric actuators [14]. It is readily incorporated into the state space model of an actuator, and due to its mathematical form can be directly used for compensation without inversion [13]. Classic implementations of the above-mentioned hysteresis models do not account for asymmetry and rate-dependence. Many variants of these models (especially of the P-I variety) have thus been developed to address these shortcomings, for example in [14–17]. The necessity of such modifications suggests an important limitation of analytical phenomenological models: the form of an analytical expression often contains implicit assumptions about the characteristics of the hysteresis which may not reflect reality. Moreover, numerical issues can arise during computation of these analytical models (e.g. Tan et al [18] show that the inverse of the P-I model can become numerically ill-conditioned.) To address these limitations, a black-box modelling method is desirable to minimise assumptions about the hysteresis or any other physical effects that may be present. Neural networks are a popular means of constructing and learning models from little *a priori* knowledge, and neural network-based controllers have been studied in detail [19–21]. Much work has been reported on the use of neural networks to build hysteresis models. Mai et al [33] propose a time-delay dynamic neural network to model hysteresis (albeit in shape-memory alloys). This is essentially a differential equation model with nonlinear mappings approximated by neural networks, and where the input signal is subject to time-delay. Experiments showed that the time-delay could be optimised to

minimise the modelling error (interestingly, [34] also shows another example where introduction of a time-delay can be beneficial).

Many approaches employ a static, feedforward neural network in combination with an auxiliary mapping. The latter is necessary because such neural networks are alone incapable of modelling dynamical behaviour like hysteresis. Therefore, the auxiliary mapping (also called a ‘hysteretic operator’ by some authors) is used to extract information about the state of the hysteresis from its input/output signals. The input space of the neural network is ‘expanded’ to include the auxiliary mapping output, and possibly other signals, along with the input to the hysteresis. Examples of this approach are the work of Zhao and Tan [22], Li and Tan [23], and Ma et al, who have proposed a variety of hysteretic operators [24–27]. Other methods in a similar direction have sought to improve accuracy, especially in accounting for rate-dependence. The model of Zhang and Tan supplements the hysteretic-operator approach with a dynamic model comprising a superposition of first-order differential operators [28]. Dang and Tan [29] use a radial basis function neural network, where the input space consists of the input and delayed output signals of the piezo actuator, and the output of their hysteretic operator, which computes an inner product from those signals. The same authors also developed a similar arrangement with a simpler mapping in [31], which is inspired by conceiving the problem as finding a nonlinear auto-regressive model with exogeneous input (NARX). In the work of Dong et al [30], the mapping computes a ‘generalised gradient’ of the hysteresis; the expanded input space is similar to Dang and Tan’s work but with the further addition of a fourth input, *viz.* the time derivative of the hysteresis input.

The above neural network-based models are not quite ‘black-box’ because their accompanying hysteretic operators may contain some rather specific assumptions about the shape of the hysteresis. It would be preferable to do away with these complicated mappings and completely rely on an appropriate neural network architecture to directly model the dynamics of the hysteresis. For the corresponding research works, see [32, 35–39].

In this paper, we propose a method for inverse modelling of a piezoelectric positioning stage using a neural network. The contributions of our work are threefold:

- The piezoelectric actuator studied here is unlike the standard stack or bender piezoelectric actuators investigated in other works. The piezoelectric motor which actuates the positioning stage enables extremely precise positioning, while enabling a great range of travel on the order of *centimetres*. As a result of its operating principle (described in Sect. 2), frictional effects are significant.
- In principle, the inverse dynamics of this actuator are position-independent and depend only on velocity and

acceleration. However, a typical approach using both these signals as inputs to a neural network inverse model results in overfitting and the resulting model is inadequate for the purpose of prediction. We show that overfitting can be avoided by identifying the dominant input variable (which was found to be *velocity*), and using only this as the input to the neural network.

- Unlike most neural network hysteresis models described above, a simple static feedforward neural network is used here, with no need for complicated hysteresis operators. This considerably simplifies implementation compared to existing methods.

The paper is organised as follows: A brief description of the piezoelectric positioning stage and experimental setup is presented in Sect. 2, and its nonlinear characteristics are investigated in Sect. 3. Construction and performance evaluation of a backpropagation neural network inverse model using both velocity and acceleration as inputs (i.e. the ‘typical’ approach) is described in Sect. 4. In Sect. 5, the neural network is designed using the dominant variable approach instead. Results demonstrating the effectiveness of this approach are presented in Sect. 6.

2 Experimental setup

The piezoelectric positioning stage investigated in this work is a PLS8 manufactured by PBA Systems. The driving method of actuator of the stage is voltage driving (See [40] for a discussion of driving piezoelectric actuators methods). The maximum range of travel of the stage is 115 mm, and the maximum velocity is 230 mm/s.

The stage is actuated by a Nanomotion HR-8 piezoelectric motor. Its working principle is briefly described (c.f. Fig. 2): The actuating elements are a set of piezoelectric ceramic fingers. The fingertips, protruding from one end of the motor, are mounted in compression against the drive belt of the work platform. When driven by electrical signals from the motor driver, ultrasonic standing waves are produced and the high frequency longitudinal extension and lateral bending of the finger generates an elliptical motion at the fingertips. The force exerted on the drive belt by the fingertips moving in such a manner produces linear motion along the direction as shown in Fig. 2. The control voltage applied to the motor driver determines the velocity of motion. In the absence of drive voltage input, the pressure of the ceramic fingertips on the drive belt maintains a holding torque on the work platform.

Position is measured by a Mercury 3000 encoder made by Celera Motion while the velocity and acceleration signals are obtained by numerical differentiation of the position. All control and measurement algorithms are implemented with

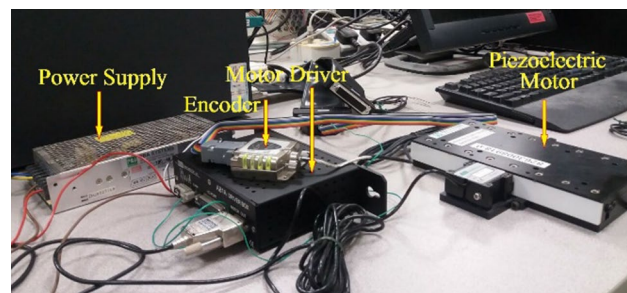


Fig. 1 The piezoelectric positioning stage system

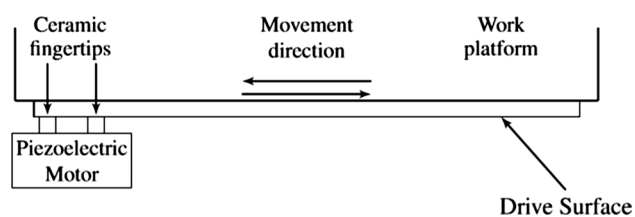


Fig. 2 Schematic illustrating the working principle of the piezoelectric positioning stage

MATLAB/SIMULINK on a host computer and executed by a dSPACE DS1104 card installed inside. Signal acquisition and generation are, respectively, via the DS1104’s 12-bit analog-to-digital converter (ADC) channels (800 ns conversion time) and 16-bit digital-to-analogue converter (DAC) channels (10 μ s settling time), both having ± 10 V dynamic range. These channels interface with the piezoelectric motor driver and the encoder. Through a user interface on the dSPACE ControlDesk software, experiments are performed with parameter adjustments and measurements made in real time. The entire piezoelectric positioning stage system is shown in Fig. 1.

3 Nonlinear characteristics of the piezoelectric positioning stage

The complexity of the nonlinear relationship between applied voltage and the resulting motion of the piezoelectric positioning stage is investigated by conducting a number of experiments.

Essential features of the voltage-velocity relationship are observed by applying a triangle waveform to the input (Fig. 3). In addition, by using a low slew rate to move the stage at low speed with minimal acceleration, it becomes reasonable to assume that the actuation force (as reflected by the applied voltage) is applied solely to overcome the frictional forces. Therefore, the relationship between frictional forces and velocity can also be inferred from Fig. 3.

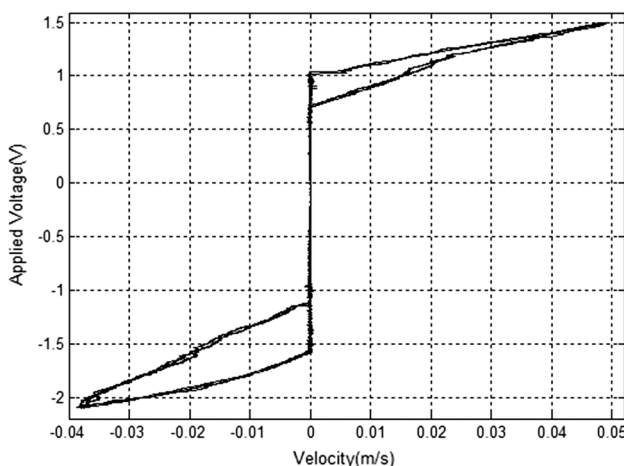


Fig. 3 Relationship between applied voltage/frictional force and velocity of the positioning stage

Apart from the presence of hysteresis, this result also suggests that Coulomb friction and viscous friction forces are significant and need to be accounted for in any model of the system. Moreover, frictional characteristics are dependent on the direction of motion.

Further complexity is revealed by applying sinusoidal signals described by the function $v = A \sin(2\pi ft - \pi/2) - 0.3$, for various values of amplitude A and frequency f . The response of the system (velocity and acceleration) is shown in Figs. 4 and 5. The results show the effects of varying frequency at a constant amplitude and the effects of varying amplitude at a constant frequency.

From the figures, it is evident that the asymmetrical hysteresis shown in Fig. 3 is a basic qualitative feature of the voltage-velocity/acceleration relationships. However,

the specific shapes of the curves depend on the temporal variation of the applied voltage, in a complicated and rather irregular manner. These results show that the motion behaviours of the piezoelectric stage have very complex nonlinear characteristics.

4 Neural network modelling—typical approach

Amongst the variety of neural networks applied in various fields of engineering, perhaps the most well-known is the feedforward neural network using the backpropagation (BP) learning algorithm (i.e. the BP neural network), which is capable of approximating any continuous nonlinear function, and is a suitable candidate for constructing an inverse model of the piezoelectric positioning stage [41].

4.1 Backpropagation neural networks

A BP neural network is a network of interconnected processing elements (i.e. neurons). Each neuron computes a weighted sum of its inputs u , which is then mapped through an activation function f to generate an output O . In this work, the hyperbolic tangent function was chosen as the activation function. Neurons are arranged in layers which are connected in cascade, such that the output of every neuron in a given layer is connected to the input of every neuron in the next (i.e. a feedforward network). The entire network comprises an input layer, an output layer, and one or more hidden layers in between. More precisely, a neuron j in the layer k computes the function given as

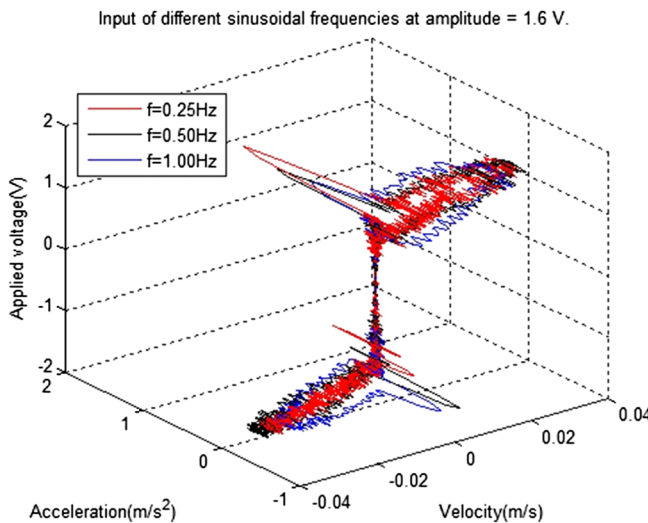
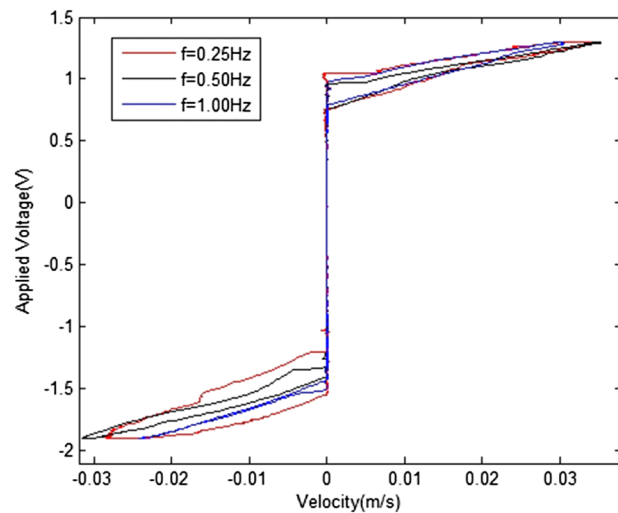


Fig. 4 Velocity and acceleration in response to sinusoidal input with amplitude 1.6V, at varying frequencies



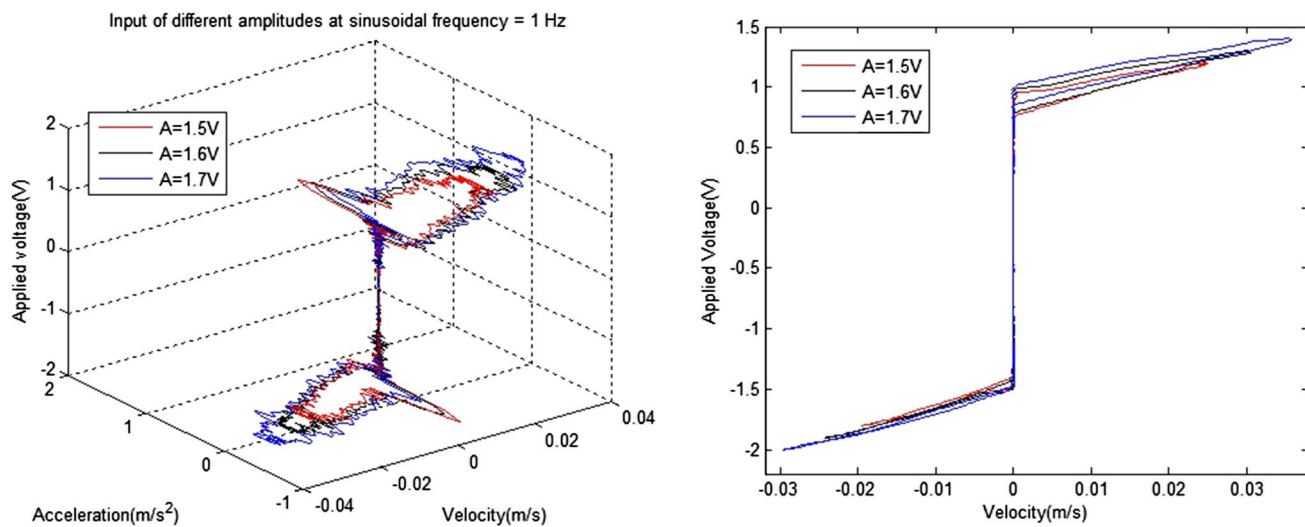


Fig. 5 Velocity and acceleration in response to 1Hz sinusoidal input at varying amplitudes

$$u_j^k = \sum_i w_{ji} O_i^{k-1} \quad (1)$$

$$O_j^k = f(u_j^k) = \frac{e^{u_j^k} - e^{-u_j^k}}{e^{u_j^k} + e^{-u_j^k}} \quad (2)$$

where w_{ji} is the weight applied to O_i^{k-1} , the output of the i -th neuron in the preceding layer ($k-1$). The outputs of the input layer O_i^0 are simply the input values presented to the network. Thus, a function is computed by the network as input signals propagate through and are transformed by successive layers from input to output. At the output layer, the output error of each neuron j , in response to a given input pattern, is the difference between the desired output D_j and its actual output O_j . During the training process, these errors are propagated back through the network in the opposite direction, and weights are adjusted accordingly in order to minimise the *overall error* of the network. A suitable measure of this is given by the instantaneous error energy e , which is a sum of squared errors of all output neurons for some input pattern given as

$$e = \frac{1}{2} \sum_j (D_j - O_j)^2 \quad (3)$$

In this work, the Levenberg–Marquardt training algorithm (a variant of classic backpropagation) is employed, with a momentum term to speed up convergence. Weights are updated at the end of every training epoch, according to the rule given by

$$\mathbf{w}_{n+1} = \mathbf{w}_n - (\mathbf{J}_n^T \mathbf{J}_n + \mu \mathbf{I})^{-1} \mathbf{J}_n^T \mathbf{e}_n + \alpha \Delta \mathbf{w}_n \quad (4)$$

where n refers to the training epoch/iteration, \mathbf{w} is a vector of all the weights in the network, \mathbf{e} is a vector of output errors, \mathbf{J} is the Jacobian matrix of the errors with respect to the weights in the network, \mathbf{I} is the identity matrix, μ is the combination coefficient and α is the momentum coefficient. The initial weights \mathbf{w}_0 are determined using the following uniform distribution [42]

$$\mathbf{w}_0 \sim U\left(-\frac{\sqrt{6}}{\sqrt{f_in + f_out}}, \frac{\sqrt{6}}{\sqrt{f_in + f_out}}\right) \quad (5)$$

where f_in is the number of connections feeding into the node, f_out is the number of connections flowing out of the node.

The operation of this algorithm is understood as an adaptive blending of the steepest gradient descent method and the Gauss–Newton method. This is controlled by the value of the combination coefficient μ which is adjusted every training iteration in order to achieve fast and stable convergence to the error minimum. Initially, μ is large and the steepest descent method dominates which gives the advantage of speed; as the error minimum is approached, μ is progressively reduced and the Gauss–Newton algorithm dominates.

Using the typical approach, a BP neural network was constructed with velocity and acceleration as the input and applied voltage as the output. It was decided to use a single hidden layer; this is premised on the well-known result that one hidden layer is sufficient to approximate any continuous function to any desired level of accuracy by selecting a suitable number of neurons. From experimental observation, it was found that a hidden layer with 120 neurons was adequate.

4.2 Training and performance

The data sets used to train and test the network are sequences of velocity and acceleration values (the inputs), paired with the corresponding control voltage values (the output). In order to collect data, the piezoelectric positioning stage is made to roughly track a sinusoidal position reference signal, using a proportional feedback position controller. At each sampling instant, the control voltage applied by the controller and the position of the stage measured by the encoder are recorded. Numerical differentiation of the position gives the corresponding velocity

and acceleration values. This process is repeated with the position reference signal set to various amplitude and frequency values. These parameter combinations are selected to span the region of operation of the piezoelectric stage, which is bounded by manufacturer-specified limits on the range of motion and operating speed. Data from two different sets of amplitude-frequency parameters are used to generate the training and test data sets, as indicated in Fig. 6. A data set is generated by concatenating one segment of data from every parameter combination used, in random order. Each segment corresponds to one cycle of the sinusoidal position reference signal and is chosen to avoid introducing jump discontinuities when concatenated with adjacent segments.

Figures 7a and 7b illustrate the performance of the neural network (after training for > 110 epochs) against the training and test data sets, respectively. The graphs plot control voltage (vertical axis) against the corresponding velocity and acceleration values (which are labelled by sequence index on the horizontal axis). The desired control voltage values generated from the training and test data sets are shown on their respective graphs in red. The actual control voltage values output by the neural network are shown in blue. It is apparent that while the neural network's output matches the training data fairly well, its performance against the test data is very poor.

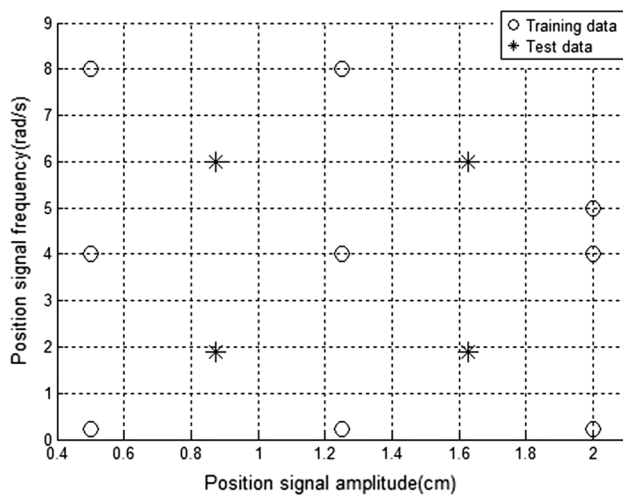


Fig. 6 Parameter combinations used to construct the training and test data sets

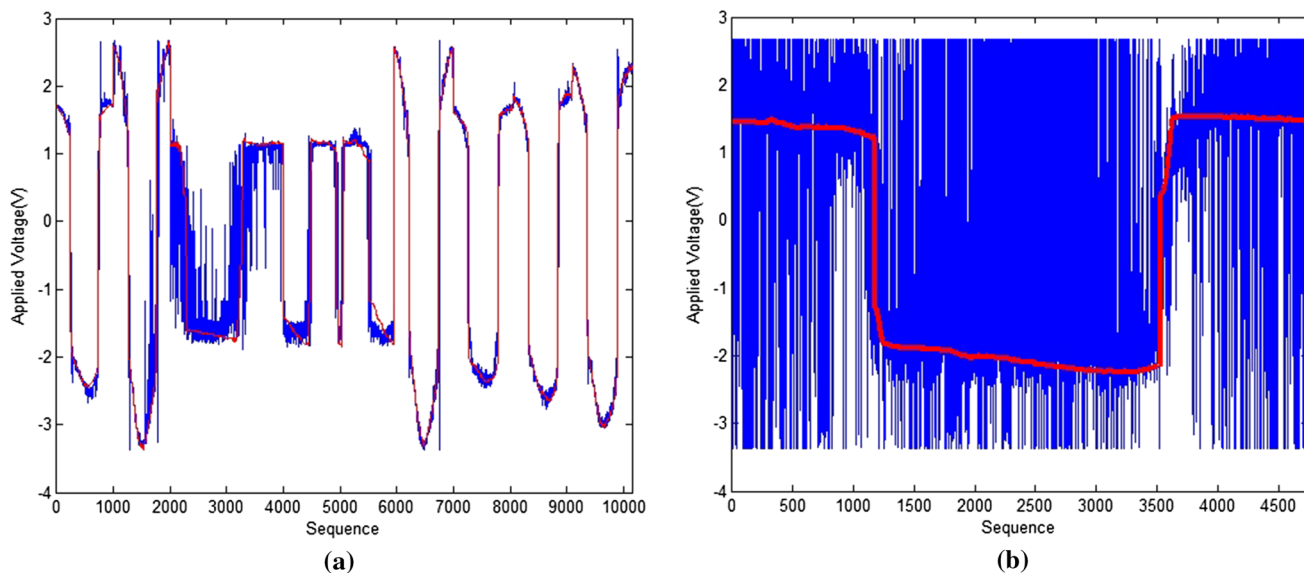


Fig. 7 Performance of the trained network constructed using the typical approach (velocity and acceleration as input and applied voltage as output)

5 Neural network modelling–dominant variable approach

It was found that the poor predictive performance of the preceding neural network inverse model could be rectified by restricting its input to only the dominant input variable of the inverse process. By ‘dominant input variable’, it is implied that the variable to which the output is most sensitive. The method of developing an approximate analytical model of the piezoelectric positioning stage dynamics is used to determine which input variable (i.e. velocity or acceleration) is dominant. The detailed modelling process of the piezoelectric positioning stage dynamics is given in the Appendix 1.

5.1 Identification of the dominant variable

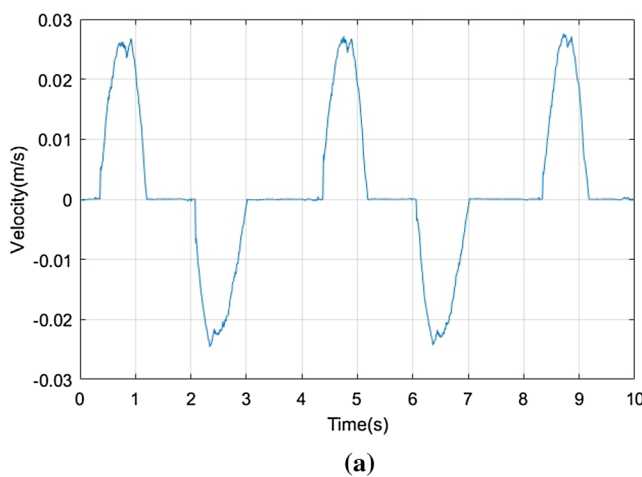
Using the modelling result of the Appendix 1, rearranging (28) to write the applied voltage u in terms of the velocity and acceleration it is obtained that

$$6u(t) = \ddot{x}(t) + a_1\dot{x}(t - 0.0035) + a_2 \operatorname{sgn}(\dot{x}(t)) \quad (6)$$

where

$$\begin{aligned} a_1 &= \begin{cases} 104.0154 \dot{x}(t - 0.0035) > 0 \\ 117.1441 \dot{x}(t - 0.0035) < 0 \end{cases} \\ a_2 &= \begin{cases} 3.1023 \dot{x}(t) > 0 \\ 6.8216 \dot{x}(t) < 0 \end{cases} \end{aligned} \quad (7)$$

The variable giving rise to terms which together make the largest contribution to the magnitude of u is considered the dominant variable. For this purpose it suffices to compare the term due to acceleration $\ddot{x}(t)$ with the term due to velocity $a_1\dot{x}(t)$ (the Coulomb friction term can be neglected because it is effectively a constant).



These terms can be evaluated by applying an input signal to the piezoelectric positioning stage and recording the resulting velocity. Fig 8a shows the velocity resulting from application of the signal $u = 1.5 \sin(\frac{\pi}{2}t - \frac{\pi}{2}) - 0.3$. From this, the value of the terms $\ddot{x}(t)$ and $a_1\dot{x}(t)$ are computed and compared (Fig 8b).

From Fig 8b the bound of $\ddot{x}(t)/a_1\dot{x}(t)$ is found to be $O(10^{-1})$, hence the output of the inverse system is dominated by its velocity.

5.2 Setting the size of the hidden layer

The neural network constructed with the new approach comprises a single neuron each in the input and output layers. The input is the velocity of the positioning stage (which was identified as the dominant variable), and the output is the applied voltage. It is, however, not straightforward to determine the appropriate number of neurons for the hidden layer, with respect to the performance of the network, since there is currently no definite rule to choosing it and it is usually determined according to the experiments and researchers’ experience [43]. The mean squared error (MSE) between the actual output y_d and predicted output y_p is used as the criterion for checking convergence of networks and can be calculated with the equation given as

$$E_{MSE} = \frac{1}{q} \sum_{i=1}^q (y_{di} - y_{pi})^2 \quad (8)$$

where q is the number of patterns presented in a data set. Using this measure, the effect of the number of hidden layer neurons on the network performance was experimentally investigated, and results are shown in Table 1.

Table 1 indicates that increasing the number of neurons in the hidden layer does not simply reduce the average MSE.

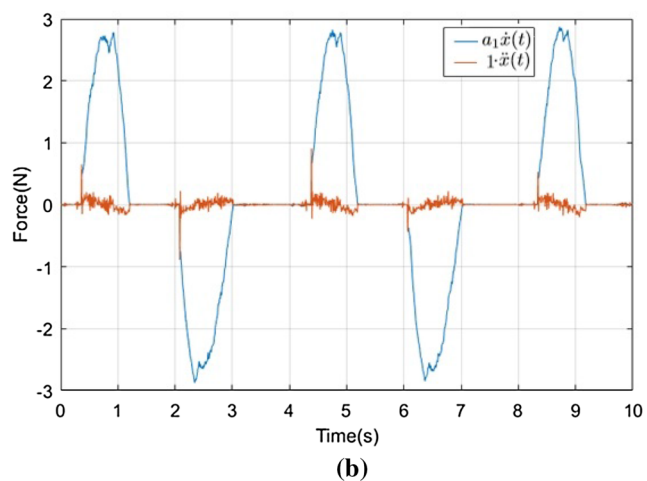


Fig. 8 Identification of the Dominant Variable

Table 1 Effect of hidden layer neurons on the network performance

Hidden layer neurons	Training epochs	Training E_{MSE}	Testing E_{MSE}
16	335	0.120776	0.054228
18	327	0.120892	0.053226
20	754	0.119935	0.053679
22	679	0.118807	0.054072
24	688	0.118161	0.052982
26	374	0.119766	0.055169
28	350	0.119977	0.053508
30	369	0.120442	0.055209
32	754	0.119834	0.054972

Rather, it appears that the optimal number of the neurons in the hidden layer is 24. The inverse model for the piezoelectric positioning stage is thus given by the neural network given as

$$y_p = \mathbf{w}_2^T f(\mathbf{w}_1^T v + \mathbf{b}_1) + b_2 \quad (9)$$

where f is the hyperbolic tangent function, v is the velocity, y_p is applied voltage, and the connection weights and biases are given as

$$\begin{aligned} \mathbf{w}_1 = & \begin{bmatrix} -35.3468 & 34.6366 & -28.435 \\ -33.44 & -33.4596 & 32.1285 \\ -29.9843 & 43.3091 & 4.3072 \\ -136.8754 & -231.9848 & 239.7699 \\ -274.3949 & 225.5036 & -224.9426 \\ -5.3267 & 44.2194 & 65.8648 \\ 33.4028 & -48.4009 & -22.5532 \\ -24.6959 & -38.4669 & 36.3986 \end{bmatrix}^T \quad (10) \end{aligned}$$

$$\begin{aligned} \mathbf{b}_1 = & \begin{bmatrix} 33.727 & -31.4364 & 23.0972 \\ 24.6802 & 22.7881 & -19.5757 \\ 15.8065 & -17.4002 & -0.49335 \\ 7.0838 & 0.00042311 & 0.27504 \\ -0.40677 & 0.84943 & -10.6875 \\ -1.408 & 17.2613 & 33.2112 \\ 29.6669 & -28.3202 & -15.6053 \\ -19.8161 & -34.0213 & 33.5377 \end{bmatrix}^T \quad (11) \end{aligned}$$

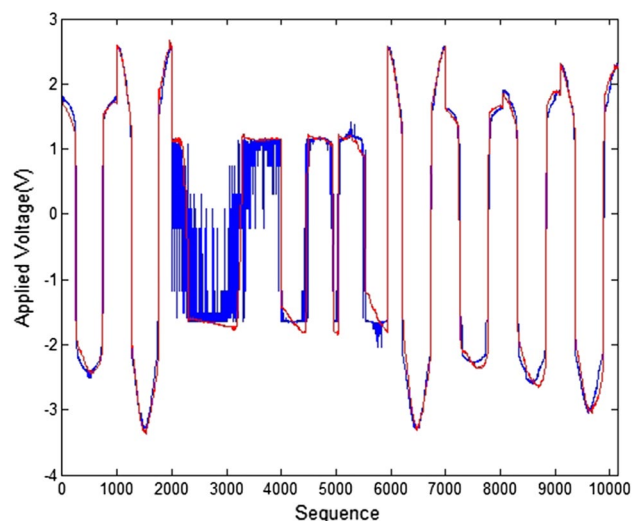


Fig. 9 Performance of the trained network constructed using the dominant variable approach (Eqn. (9)). (Neural network output in blue, training data set in red.)

$$\mathbf{w}_2 =$$

$$\begin{bmatrix} -0.16523 & 0.10884 & -0.1075 \\ -0.034101 & -0.051026 & 0.024077 \\ -0.074166 & 0.037539 & 0.1368 \\ -0.066009 & -32.9146 & -85.532 \\ -44.7181 & 8.3888 & -0.10717 \\ -0.06488 & 0.040388 & 0.041598 \\ -3.6387 & -0.035379 & -0.10142 \\ -0.13976 & -3.1364 & 0.75016 \end{bmatrix}^T \quad (12)$$

$$b_2 = 0.0072113 \quad (13)$$

The performance of the neural network against the training data set after 688 epochs (c.f. Table 1) is shown in Fig. 9.

6 Prediction performance of the neural network model based on the dominant variable approach

The prediction performance of the neural network was evaluated in two ways, first by checking its output against measured behaviour (i.e. with the test data set), and second by its effectiveness in providing feedforward compensation to a PI controller for position tracking. The results are as follows:

6.1 Prediction performance with test data set

Figure 10 shows the outputs of the neural network (9) (dashed lines) and the approximate analytical model (6)

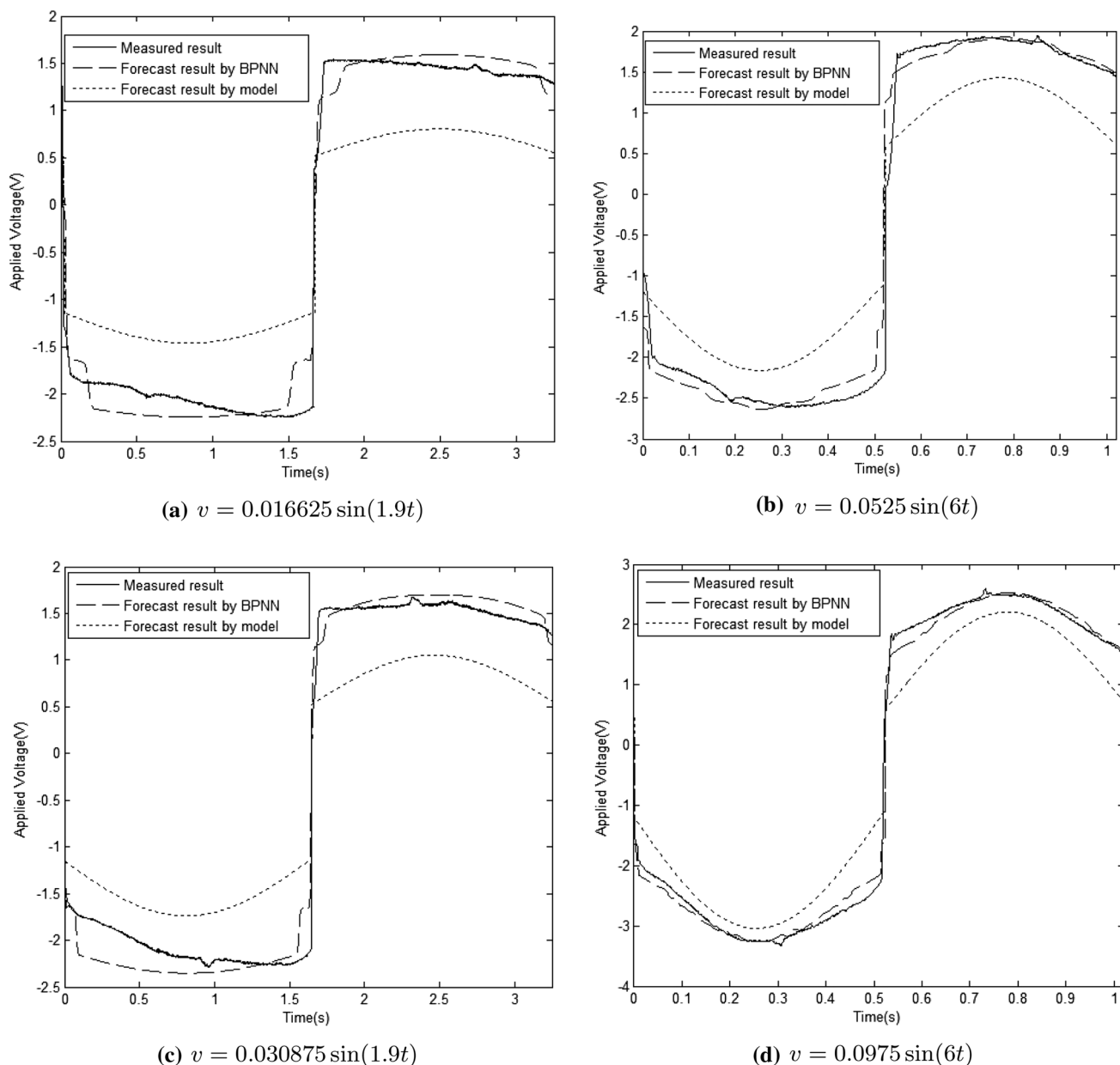


Fig. 10 Comparison of predictions of the neural network model using the dominant variable approach, and the analytical model, with the test data set

(dotted lines) in response to each of the four signals comprising the test data set (c.f. Fig. 6). The results indicate that the neural network's predictions are in fairly good agreement with actual behaviour and are much more accurate than the analytical model.

6.2 Prediction performance with other input waveforms

Prediction performance of the neural network was further validated by another set of data, generated in the same

manner as described in sect. 4.2, but using approximate triangular and square position reference signals instead. (These signals were approximated with sinusoids in order to avoid exceeding the maximum permissible velocity of the piezoelectric stage when collecting measurement data.) Likewise, results in Fig. 11 indicate better performance compared with the analytical model.

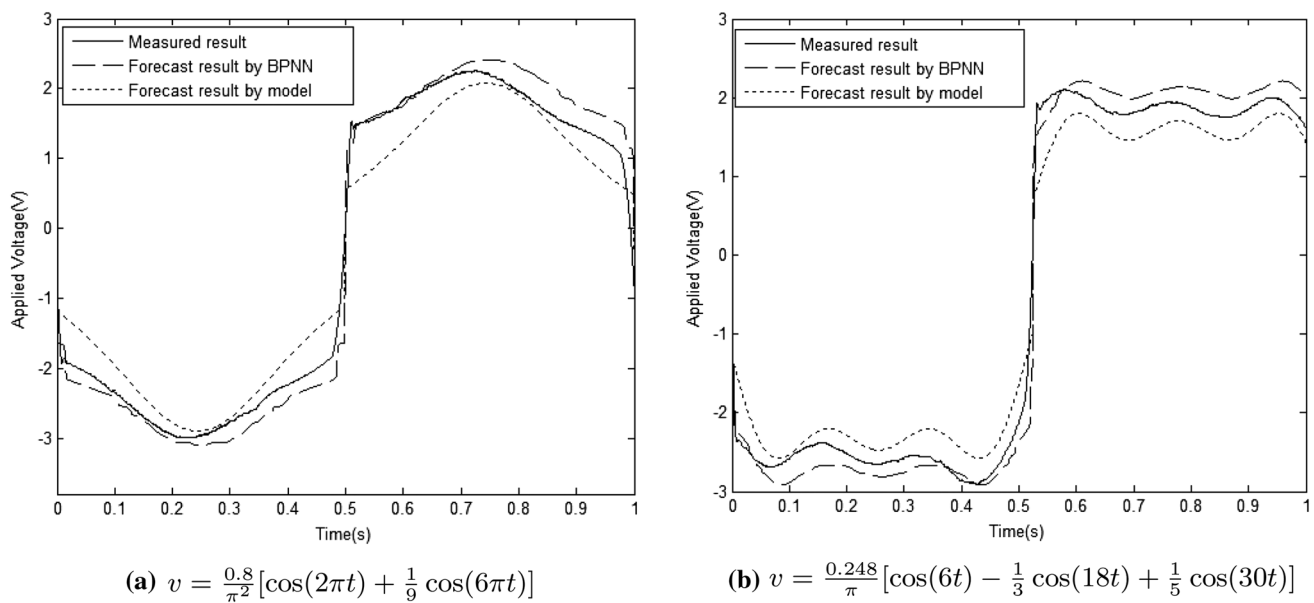


Fig. 11 Further comparison of predictions of the neural network model using the dominant variable approach and the analytical model

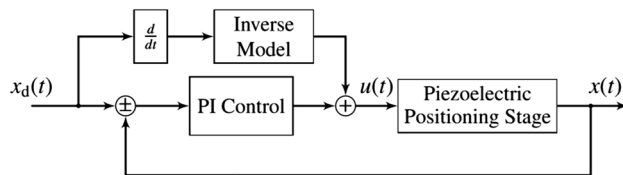


Fig. 12 Block diagram of PI position controller with neural network feedforward compensation

6.3 Prediction performance in feedforward compensation

The effectiveness of the inverse neural network model for feedforward compensation was evaluated by comparing the position tracking performance of a PI controller alone, and with feedforward compensation using either the approximate analytical model or the neural network (see Fig. 12 for block diagram). The position signal to be tracked is shown in Fig. 13, and a similar signal at a higher frequency of 1.0Hz is also used. PI controller gains were adjusted (in the absence of feedforward compensation) in order to achieve minimal tracking error without oscillation, resulting in a proportional gain of 19000 and an integral gain of 660000. A comparison of the tracking errors and control signals generated by the PI controller alone, and with each type of feedforward compensation, is shown in Figures 14 and 15, respectively.

As was discussed earlier, for the piezoelectric position stage, the frictional disturbance influences the dynamics of the system greatly and, therefore, it is expected that the

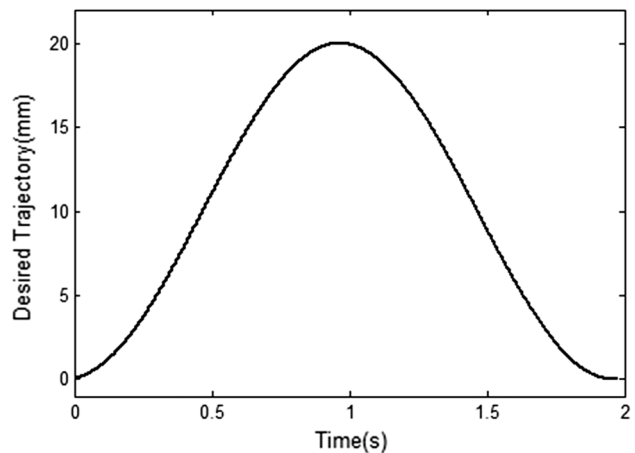


Fig. 13 Position reference signal to be tracked

tracking would suffer at low speeds. From Fig. 14, it is seen that error is greatest at the onset of motion and attenuates once the stage is in motion. Even though integral action is capable of attenuating the effects of the disturbance, the PI controller on its own is unable to react quickly enough. As it would be expected, the performance with feedforward compensation would be better because of the instantaneous compensation of the frictional disturbance. The results of Fig. 14 demonstrate that use of the neural network inverse model for feedforward compensation can greatly improve the position control accuracy of the piezoelectric positioning stage because of the higher accuracy in the model compared to the approximate model.

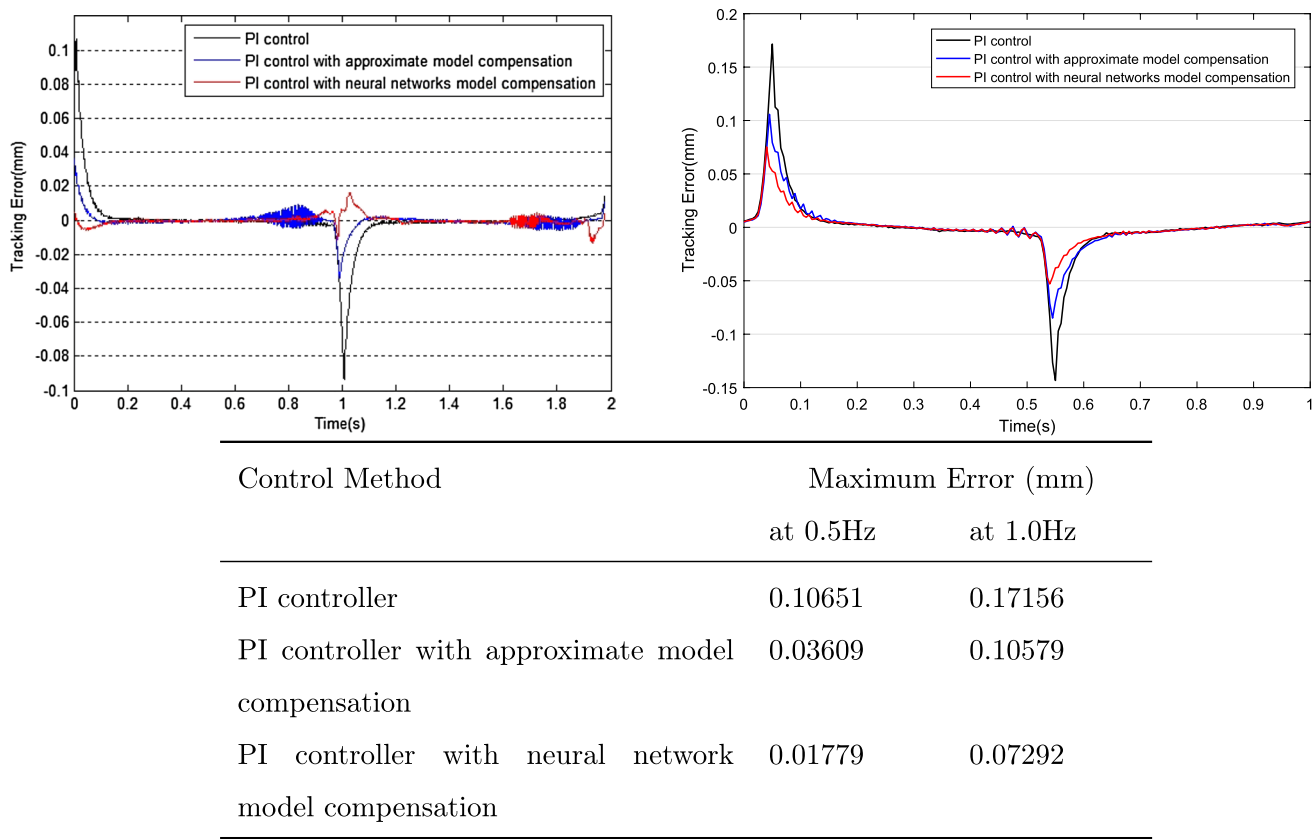


Fig. 14 Comparisons of the tracking error of the controller using various compensation schemes, at different reference signal frequencies (0.5Hz at left, 1.0Hz at right)

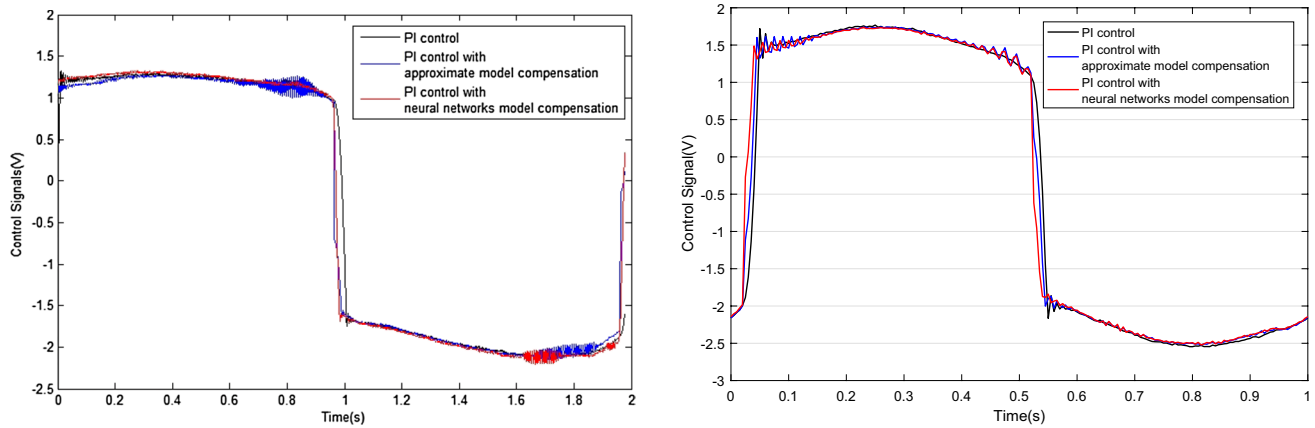


Fig. 15 Comparisons of the control signals generated by the controller using various compensation schemes, at different reference signal frequencies (0.5Hz at left, 1.0Hz at right)

7 Conclusions

An approach for developing a neural network inverse model of a piezoelectric positioning stage, which exhibits

rate-dependent, asymmetric hysteresis has been presented. The difficulties in modelling piezoelectric actuators have been discussed, and various approaches have been compared to the proposed approach. It was shown that the dominant variable approach to neural network design is

capable of producing better prediction results as compared to classical approaches. Furthermore, the use of this dominant variable inverse model as a feedforward compensator in conjunction with a PI position controller demonstrated much better tracking performance with lower error compared to compensation using the approximate analytical model.

Appendix 1: Approximate analytical model of the piezoelectric positioning stage

Despite the complexity of the mechanism, with a little physical intuition, it is possible to obtain a rough analytical model that suffices the purpose of identifying the dominant variable. Considering that the piezoelectric positioning stage consists of a platform that slides on rigid rails, friction is expected to play a major role in the disturbances affecting the system's performance. Classical models of friction are constructed by various combinations of Coulomb, viscous, and drag friction as their basic components. A brief review of the various types of frictional forces and their mathematical representation is as follows:

Frictional effects

Coulomb Friction Coulomb friction is a type of mechanical damping in which energy is consumed during sliding motion. The frictional force resulting from the relative motion of two surfaces in mutual contact always acts opposite to the relative motion and is proportional to the normal force of contact. It is simply given as

$$F_c = f_c \operatorname{sgn}(\dot{x}) \quad (14)$$

where f_c is the normal force.

Viscous Friction Viscous friction arises from the motion of any object through or past another object, and acts against this motion. Under well-lubricated conditions, the viscous frictional force is approximately proportional to velocity. It is characterised by the following linear relationship given as

$$F_v = f_v \dot{x} \quad (15)$$

where f_v is the coefficient of viscous friction.

Drag Friction Drag friction is the frictional force on a solid object moving through a fluid. It is proportional to the square of the velocity given by

$$F_d = f_d \dot{x} |\dot{x}| \quad (16)$$

where f_d is the drag coefficient.

As the results of Sect. 3 suggest, viscous and Coulomb friction effects are significant and should be accounted for in the model. On the other hand, drag friction can be neglected due

to the low speed of motion of the stage and its low drag coefficient in air.

Parameter identification

Besides friction, the other major force acting on the piezoelectric position stage is the force provided by the actuator. On the basis of the manufacturer's specifications, this is assumed to be a linear function of the applied voltage. Therefore, according to Newton's second law, the dynamics of the piezoelectric positioning stage can be described by the following second-order differential equation given as

$$\ddot{x} = -\frac{k_1}{m} \dot{x} - \frac{k_2}{m} \operatorname{sgn}(\dot{x}) + \frac{k_3}{m} u \quad (17)$$

where m denotes the rotor mass of piezoelectric positioning stage, k_1 and k_2 are, respectively, the viscous and Coulomb frictional coefficients, u is the input voltage and k_3 is the constant relating voltage to actuator force.

For notational convenience, and to emphasise that the frictional coefficients depend on the direction of motion (c.f. Sect. 3), re-write the coefficients in this manner as

$$\begin{aligned} a_1 &= \frac{k_1}{m} = \begin{cases} a_{1p} & \dot{x} > 0 \\ a_{1n} & \dot{x} < 0 \end{cases} \\ a_2 &= \frac{k_2}{m} = \begin{cases} a_{2p} & \dot{x} > 0 \\ a_{2n} & \dot{x} < 0 \end{cases} \\ a_3 &= \frac{k_3}{m} \end{aligned} \quad (18)$$

According to manufacturer specifications, $a_3 = 6 \frac{N}{V \cdot kg}$. To obtain the values of the remaining parameters in (A.4), the stage is driven in both directions by subjecting it to a variety of positive and negative voltage pulses of duration 0.4s.

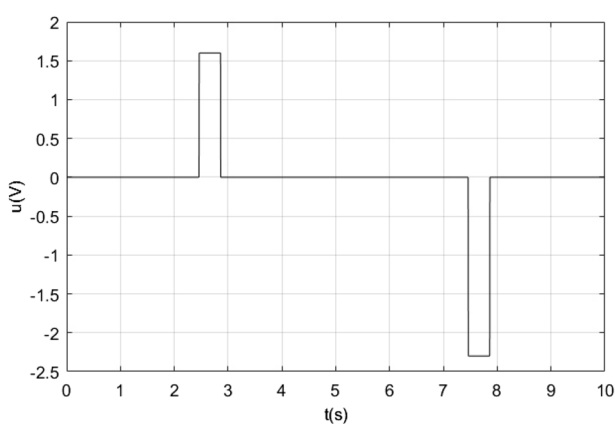
Applying pulses of 1.6 and $-2.3V$ amplitude and recording the resulting velocity of the positioning stage as shown in Fig. 16, the following expressions are obtained that

$$\begin{cases} 0.05562a_{1n} + a_{2n} - 2.3 \times 6 = 0 \\ -0.06222a_{1p} - a_{2p} + 1.6 \times 6 = 0 \end{cases} \quad (19)$$

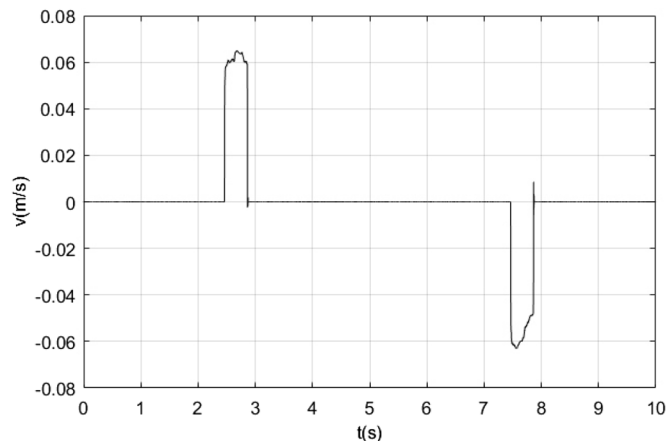
Following a similar method, using pulses of similar duration (0.4s) and various amplitudes of $-1.8V$, $1.3V$, $-2V$, $1.5V$, $-2.1V$, $1.7V$, $-2.5V$, $2V$, respectively, it is obtained that

$$\begin{cases} 0.03393a_{1n} + a_{2n} - 1.8 \times 6 = 0 \\ -0.04465a_{1p} - a_{2p} + 1.3 \times 6 = 0 \end{cases} \quad (20)$$

$$\begin{cases} 0.04622a_{1n} + a_{2n} - 2.0 \times 6 = 0 \\ -0.05742a_{1p} - a_{2p} + 1.5 \times 6 = 0 \end{cases} \quad (21)$$



(a) Pulses applied.



(b) Velocity of the positioning stage.

Fig. 16 Application of voltage pulses 0.4s duration, with amplitudes of 1.6 and -2.3V , respectively, and resulting velocity of the positioning stage

$$\begin{cases} 0.04991a_{1n} + a_{2n} - 2.1 \times 6 = 0 \\ -0.06863a_{1p} - a_{2p} + 1.7 \times 6 = 0 \end{cases} \quad (22)$$

$$\begin{cases} 0.07120a_{1n} + a_{2n} - 2.5 \times 6 = 0 \\ -0.08519a_{1p} - a_{2p} + 2.0 \times 6 = 0 \end{cases} \quad (23)$$

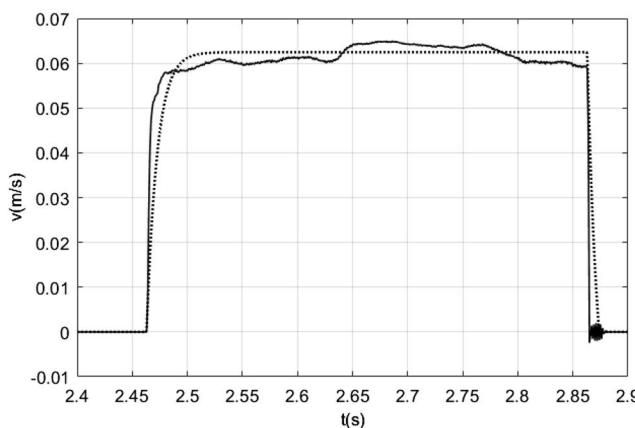
Using the method of least squares, let

$$\mathbf{a} = [a_{1p} \ a_{1n} \ a_{2p} \ a_{2n}]^T \quad (24)$$

$$\mathbf{y} = [10.8 \ 12 \ 12.6 \ 13.8 \ 15 \ -7.8 \ -9 \ -9.6 \ -10.2 \ -12]^T \quad (25)$$

and \mathbf{x} be the coefficients of \mathbf{a} , and solve equation (26) as

$$\mathbf{a} = (\mathbf{x}^T \mathbf{x})^{-1} \mathbf{x}^T \mathbf{y} \quad (26)$$



Thus, the values for $a_{1p}, a_{1n}, a_{2p}, a_{2n}$ are obtained as

$$\begin{cases} a_{1p} = 104.0154 \\ a_{1n} = 117.1441 \end{cases} \quad \begin{cases} a_{2p} = 3.1023 \\ a_{2n} = 6.8216 \end{cases} \quad (27)$$

To verify these values, they were substituted into (27) to compute the velocity of the positioning stage in response to applied voltage pulses of amplitude 1.6V and -2.3V . Figure 17 shows a comparison of the velocity computed from the model (dotted line) to the actual response of the system (solid line).

From Fig. 17, it is seen that the frictional force in (17) appears delayed by about 0.0035s compared to the actual behaviour. The viscous friction term in (17) is adjusted to correct for this, in order to achieve a better match between the modelled and actual velocities, as shown in Fig. 18. Therefore, the dynamical model is obtained as

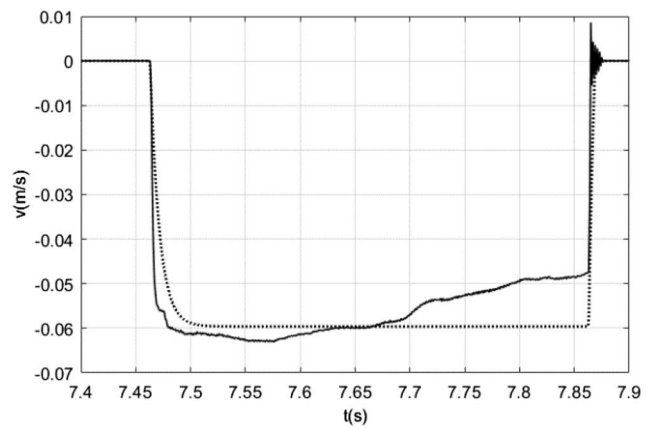


Fig. 17 Comparison of the velocity computed using (dotted line) with the actual response of the system (solid line), in response to input pulses of 0.4s duration, with amplitudes of 1.6V and -2.3V , respectively

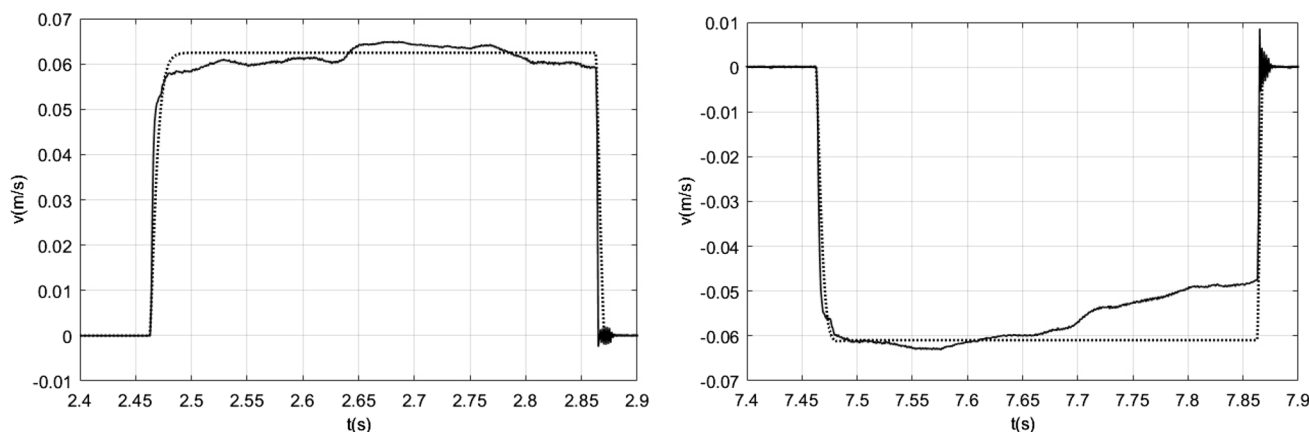


Fig. 18 Comparison of the velocity computed using the model (dotted line) with the actual response of the system (solid line), under the same conditions as those for which Fig. 17 are obtained, after adjustments to the viscous friction term

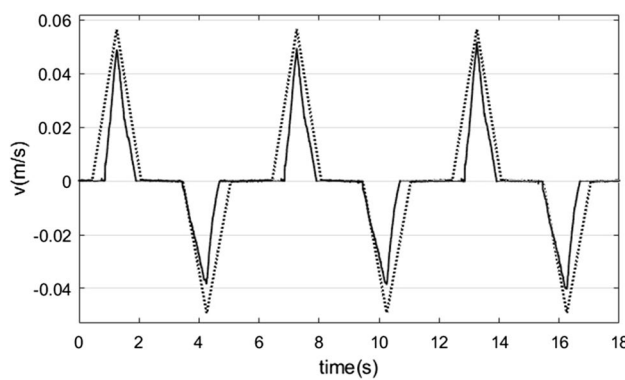


Fig. 19 Comparison of the velocity computed using the model (dotted line) with the actual response of the system (solid line), in response to a triangle function input of 6 second period and peak amplitudes at 1.5 and -2.1V

$$\ddot{x}(t) = -a_1 \dot{x}(t - 0.0035) - a_2 \operatorname{sgn}(\dot{x}(t)) + 6u(t) \quad (28)$$

where

$$a_1 = \begin{cases} 104.0154 & \dot{x}(t - 0.0035) > 0 \\ 117.1441 & \dot{x}(t - 0.0035) < 0 \end{cases} \quad (29)$$

$$a_2 = \begin{cases} 3.1023 & \dot{x}(t) > 0 \\ 6.8216 & \dot{x}(t) < 0 \end{cases}$$

To verify this model, a comparison is made between the simulated and actual velocities of the piezoelectric stage in response to a triangular function input with a period of 6 seconds and peak amplitudes at 1.5 V and -2.1V (see Fig. 19, dotted line shows velocity computed with the model, solid line shows velocity measured from actual system). It can be seen that although the model is not accurate, the results are in qualitative agreement with the actual system,

and this is sufficient for the purpose of identifying the dominant variable.

References

- Chang SH, Tseng CK, Chien HC (1999) "An ultra-precision XY θ_Z piezo-micropositioner. Part II. Experiment and performance" IEEE Transactions on Ultrasonics, Ferroelectrics, and Frequency Control, 46(4), 906-912
- Croft D, Shedd G, Devasia S (2000) "Creep, hysteresis, and vibration compensation for piezoactuators: atomic force microscopy application," Proceedings of the 2000 American Control Conference, 3, 2123-2128
- Song H, Vdovin G, Fraanje R, Schitter G, Verhaegen M (2009) Extracting hysteresis from nonlinear measurement of wavefront-sensorless adaptive optics system. Opt Lett 34(1):61-63
- Yang W, Lee SY, You BJ (2010) A piezoelectric actuator with a motion-decoupling amplifier for optical disk drives. Smart Mater Struct 19(6):065027
- Mohammadzaheri M, Alqallaf A (2017) Nanopositioning Systems with Piezoelectric Actuators, Current State and Future Perspective. Sci Adv Mater 9(7):1071-1080
- Yan GF, Fang H, Meng F (2019) High-accuracy tracking of piezoelectric positioning stage by using iterative learning controller plus PI control. J Braz Soc Mech Eng 41:1-9
- Xu Q, Tan KK, (2016) Advanced Control of Piezoelectric Micro-/ Nano-Positioning Systems
- Mohammadzaheri M, Grainger S, Bazghaleh M (2013) A system identification approach to the characterization and control of a piezoelectric tube actuator. Smart Mater Struct 22(10):105022
- Mohammadzaheri M, Grainger S (2012) A comparative study on the use of black box modelling for piezoelectric actuators. Int J Adv Manuf Technol 63(9):1247-1255
- Hassani V, Tjahjowidodo T, Do TN (2014) A survey on hysteresis modeling, identification and control. Mech Syst Signal Process 49(1-2):209-233
- Song Xianfeng, Duggen L, Lassen B, Mangeot C (2017) "Modeling and identification of hysteresis with modified Preisach model in piezoelectric actuator," 2017 IEEE International Conference on Advanced Intelligent Mechatronics (AIM), Munich, pp. 1538-1543

12. Al Janaideh M, Rakheja S, Su C (2011) An Analytical Generalized Prandtl-Ishlinskii Model Inversion for Hysteresis Compensation in Micropositioning Control. *IEEE/ASME Trans Mech* 16(4):734–744
13. Rakotondrabe M (2011) Bouc-Wen Modeling and Inverse Multiplicative Structure to Compensate Hysteresis Nonlinearity in Piezoelectric Actuators. *IEEE Trans Auto Sci Eng* 8(2):428–431
14. Shunli Xiao, Yangmin Li (2014) Dynamic compensation and H_{∞} control for piezoelectric actuators based on the inverse Bouc-Wen model. *Robotics and Computer-Integrated Manufacturing* 30(1):47–54
15. Ang WT, Khosla PK, Riviere CN (2007) Feedforward Controller With Inverse Rate-Dependent Model for Piezoelectric Actuators in Trajectory-Tracking Applications. *IEEE/ASME Trans Mechatron* 12(2):134–142
16. Gu G, Zhu L, Su C (2014) Modeling and Compensation of Asymmetric Hysteresis Nonlinearity for Piezoceramic Actuators With a Modified Prandtl-Ishlinskii Model. *IEEE Trans Ind Electron* 61(3):1583–1595
17. Li Z, Su C, Chen X (2014) Modeling and inverse adaptive control of asymmetric hysteresis systems with applications to magnetostrictive actuator. *Control Eng Pract* 33:148–160
18. Tan U et al (2009) Feedforward controller of Ill-conditioned hysteresis using singularity-free prandtl-ishlinskii model. *IEEE/ASME Trans Mechatron* 14(5):598–605
19. Hunt KJ, Irwin G, Warwick K (1995) Neural Network Engineering in Dynamic Control Systems. Springer, New York
20. Narendra KS (1996) Neural networks for control theory and practice. Proceed IEEE 84(10):1385–1406
21. Ge SS et al (2002) Stable Adaptive Neural Network Control. Springer, New York
22. Zhao X, Tan Y (2006) Neural network based identification of Preisach-type hysteresis in piezoelectric actuator using hysteretic operator. *Sensors Actuators A: Phys* 126(2):306–311
23. Chuntao L, Yonghong T (2004) A neural networks model for hysteresis nonlinearity. *Sensors Actuators: A Phys* 112(1):49–54
24. Ma L, Tan Y, Chu Y (2008) Improved EHM-based NN hysteresis model. *Sensors Actuators A: Phys* 141(1):6–12
25. Ma L, Tan Y, Shen Y (2011) A neural networks based model of inverse hysteresis. *Phys B: Phys Condens Matter* 406(21):4109–4114
26. Ma L et al (2014) A modified HO-based model of hysteresis in piezoelectric actuators. *Sensors Actuators A: Phys* 220:316–322
27. Ma L et al (2016) Modeling hysteresis for piezoelectric actuators. *J Intell Mater Syst Struct* 27(10):1404–1411
28. Zhang X, Tan Y (2010) A hybrid model for rate-dependent hysteresis in piezoelectric actuators. *Sensors Actuators: A Phys* 157(1):54–60
29. Dang X, Tan Y (2005) An inner product-based dynamic neural network hysteresis model for piezoceramic actuators. *Sensors Actuators: A Phys* 121(2):535–542
30. Dong R, Tan Y, Chen H, Xie Y (2008) A neural networks based model for rate-dependent hysteresis for piezoceramic actuators. *Sensors Actuators A: Phys* 143(2):370–376
31. Dang X, Tan Y (2007) RBF neural networks hysteresis modelling for piezoceramic actuator using hybrid model. *Mech Syst Signal Process* 21(1):430–440
32. Li W, Chen X (2013) Compensation of hysteresis in piezoelectric actuators without dynamics modeling. *Sensors Actuators A: Phys* 199:89–97
33. Mai H, Song G, Liao X (2016) Time-delayed dynamic neural network-based model for hysteresis behavior of shape-memory alloys. *Neural Comput Appl* 27(6):1519–1531
34. Ai B et al (2016) Stability and Performance Analysis of Time-Delayed Actuator Control Systems. *J Dyn Syst, Measurement, Control* 138(5):051005
35. Liu X, Xiu C (2007) Hysteresis modeling based on the hysteretic chaotic neural network. *Neural Comput Appl* 17(5):579–583
36. Laudani, A, Lozito GM, Fulginei FR, Salvini A (2016) Modeling dynamic hysteresis through Fully Connected Cascade neural networks. 2016 IEEE 2nd International Forum on Research and Technologies for Society and Industry Leveraging a better tomorrow (RTSI), Bologna pp. 1–5
37. Deng L, Seethaler RJ, Chen Y, Yang P, Cheng Q (2016) “Modified Elman neural network based neural adaptive inverse control of rate-dependent hysteresis.” 2016 International Joint Conference on Neural Networks (IJCNN). BC, Vancouver, pp 2366–2373
38. Deng L, Tan Y (2009) Modeling hysteresis in piezoelectric actuators using NARMAX models. *Sensors Actuators: A Phys* 149(1):106–112
39. Xu Q (2013) Identification and Compensation of Piezoelectric Hysteresis Without Modeling Hysteresis Inverse. *IEEE Trans Ind Electron* 60(9):3927–3937
40. Bazghaleh M, Grainger S, Mohammadzaheri M (2018) A review of charge methods for driving piezoelectric actuators. *J Intell Mater Syst Struct* 29(10):2096–2104
41. Mohammadzaheri M, Lei C, Grainger S (2012) A critical review of the most popular types of neuro control. *Asian J Control* 14(1):1–11
42. Bengio Y, Glorot X (2010) Understanding the difficulty of training deep feed forward neural networks. *Proc, AISTATS*
43. Sun X, Long C, Jiang H et al (2016) High-Performance Control for a Bearingless Permanent-Magnet Synchronous Motor Using Neural Network Inverse Scheme Plus Internal Model Controllers. *IEEE Trans Industr Electron* 63(6):3479–3488

Publisher's Note Springer Nature remains neutral with regard to jurisdictional claims in published maps and institutional affiliations.